Micromechanical Properties of the Annulus Fibrosus in the Disc: Effect of Chronic Disease

By

Nelufer Kuzhimpadath

Thesis
Submitted to Flinders University
for the degree of

Master of Engineering (Biomedical)

College of Science and Engineering, Flinders University
23 May 2024

TABLE OF CONTENTS

ABSTRACT

Diabetes is a chronic disease and is one of the main contributing factors to lower back pain and degeneration of the disc in the world. Diabetes promotes advanced glycation end products (AGEs) to accumulate in the body, which causes disruption of the structural composition of the intervertebral discs (IVDs). The accumulation process of AGEs is accelerated due to diabetes. Numerous studies in animals have been conducted on how the properties of the IVD are affected by diabetes leading to its failure by inducing glycation artificially in them. However, only two studies focusing on how diabetes affects the IVD's annulus fibrosus (AF) have been completed. Therefore, the gap in the literature is that studies have only been conducted on animal models, the glycation was induced artificially, and there is very little research done on the effects of diabetes on the AF.

The main aim of this research study is to investigate how the micromechanical properties of the AF are affected by diabetes in human cadaver AF samples between the control and diabetic groups. This study was carried out using the methodology adapted from Tavakoli and Costi, 2018, where micromechanical testing was conducted at three different strain rates of $0.1\ \%s^{-1}, 1\ \%s^{-1}, and\ 10\ \%s^{-1}$, which are slow, medium, and fast test rates, respectively. After that, the specimen was subjected to a failure test of strain rate $10\ \%s^{-1}$. Tests were conducted in both tensile and shear loading directions on the CellScale BioTester machine (CellScale, Waterloo, Ontario, Canada).

The results obtained were in terms of stiffness and hysteresis loss coefficient from the non-destructive dynamic tests and peak load and energy absorbed at failure from the destructive or failure test. The specimens were exhibiting viscoelastic behaviour in both loading directions. The specimens showed higher stiffness in the diabetic group compared to the healthy specimens in the tensile direction, and the peak load at failure was approx. 30% lower for diabetic specimens in the shear direction as they are more prone to failure. The gap in the literature is bridged by conducting this study on diabetic human cadaver samples instead of animal models, and the results from this study can give a better understanding of how diabetes affects the micromechanical properties of the AF. This study can provide more in-depth knowledge and contribute to developing better techniques to help the affected patients and make their lives better.

DECLARATION

I certify that this thesis:

1. does not incorporate without acknowledgment any material previously submitted for a degree or diploma in any university

2. and the research within will not be submitted for any other future degree or diploma without the permission of Flinders University; and

3. to the best of my knowledge and belief, does not contain any material previously published or written by another person except where due reference is made in the text.

Signature of student....*Nelufer*.....................................

Print name of student......NELUFER KUZHIMPADATH...................................

Date......16/07/2024..................................

I certify that I have read this thesis. In my opinion it is/is not (please circle) fully adequate, in scope and in quality, as a thesis for the degree of Master of Engineering (Biomedical). Furthermore, I confirm that I have provided feedback on this thesis and the student has implemented it minimally/partially/fully (please circle).

Signature of Principal Supervisor..

Print name of Principal Supervisor..

Date..

ACKNOWLEDGEMENTS

First of all, I would like to express my sincerest gratitude to my primary thesis supervisor, Associate Professor John J. Costi, for guiding and mentoring me throughout my master's thesis. His guidance gave me the confidence to pursue my research study through to the very end. He has always taken time out of his busy and hectic schedule to reply to my queries and concerns and provide constructive feedback. I would also like to express my sincere thank you to my secondary thesis supervisor, Mr. Michael P. Russo, for his incomparable patience, continuous support, and extremely valuable knowledge. He was always present to guide and help me through the difficulties I faced in the laboratory. I will always be thankful to both my supervisors for their knowledge and time.

I would also like to extend my sincere thanks to my dear friend Abraham Jacob for taking time to train me in the lab and help me familiarise myself with the testing setup and experimental techniques, for always being available to clear my doubts and concerns, and for providing continuous moral support and confidence.

I would like to express my heartfelt gratitude to my family and friends for their unconditional love, support, and prayers, which have made me come so far in this journey. I would also like to thank my friend Natasha for being there with me in the lab during my thesis and giving me confidence and encouragement.

LIST OF FIGURES

LIST OF TABLES

INTRODUCTION

Diabetic mellitus is a chronic disease, also known as a metabolic disorder (Sapra and Bhandari, 2022), affecting a large portion of the world population. Diabetes has been shown to affect the intervertebral discs (IVDs) adversely, in particular the fibre-reinforced tissues or fibrous connective tissues, such as the annulus fibrosus (AF), present in the IVDs. This is mainly because they experience larger and more complex loads during everyday activities when compared to other joints and bones present in the body (Chan et al., 2011). The results of research studies conducted by Buckwalter, 1995 and Luoma et al., 2000 reported that prolonged and repeated loading can cause mechanical failure, structural disruption, and damage to the IVDs, which in turn results in discomfort and pain during movement, causing reduced and limited mobility of the body (Buckwalter, 1995; Luoma et al., 2000).

According to the International Diabetes Federation's (IDF) 2021 statistics, every one in ten people, which is a total of 537 million people worldwide, are living with diabetes mellitus, and the majority of them are in the western Pacific region (206 million). This is predicted to increase to 643 million people worldwide by the year 2030, and by the year 2045, it will increase to 783 million, which is a 46% increase (International Diabetes Federation, 2021). In accordance with the IDF 2021 statistics, diabetes and its related adverse long-term repercussions affect a large number of the world population, which in turn results in an increase in the economic burden due to the related medical expenses.

The structural properties and composition of the IVD can change due to ageing and various other diseases, which in turn alters the mechanical properties and damages the IVDs and the surrounding structures and tissues, as reported from the studies conducted by Urban and Roberts, 2003, and Adams and Roughley, 2006 (Urban and Roberts, 2003; Adams and Roughley, 2006). Jhawar et al., 2006 stated that diabetes is one of the primary cardiovascular risk factors because of its relatively high risk of accelerating IVD degeneration (Jhawar et al., 2006).

Research studies conducted by Lintz et al., 2022 and Werbner et al., 2022 reported that the presence of diabetes in the body speeds up the process of accumulating advanced glycation end products (AGEs). AGEs are end products of a non-enzymatic reaction between free reducing sugars and amino acids called the glycation process happening in the tissues, and this leads to the IVD degeneration process being accelerated (Lintz et al., 2022; Werbner et al., 2022). When there is an injury or disruption to the structural composition of the IVD,

degeneration can be induced or accelerated. Degeneration, in turn, can cause annular tears in the AF and disrupt the structural composition of the IVD (Castro et al., 2022). Results from research studies conducted by Mantyselka et al., 2008 and Takahashi et al., 2013 show that there is a connection between diabetes and increased incidence of lower back pain and its severity, and there is also a link between disorders related to IVD degeneration and diabetes (Mantyselka et al., 2008; Takahashi et al., 2013).

Since the prevalence of lower back pain has increased due to the ageing population and an increasing incidence of the diabetes epidemic globally, there has been an increased requirement for lower back pain management in recent years (Bloom et al., 2011). The research studies mentioned above have only looked into tendons, cartilages, and IVD as a whole disc but not much on how diabetes effects the AF. Till date, only two studies have been conducted that focus on how diabetes affects the AF; the studies were conducted on bovine samples, and they were performed by Werbner et al., 2022 and Zhou et al., 2023. These two studies are by the same group of researchers, and the latter study is the continuation of the first. Therefore, this research study aims to understand how diabetes affects the micromechanical properties of the human AF, as very little research has been conducted in this area. The methodology for this study has been adapted from the study conducted by Tavakoli and Costi, 2018 on the inter-lamellar matrix in the AF to determine their mechanical characteristics at the micro level and nano level (Tavakoli and Costi, 2018). The gap in the literature is that only animal models with artificially induced glycation have been used for research, and studies have not been particularly focused on the AF. Hence, this study will be conducted on human cadaver AF samples between the control and diabetic groups to compare the micromechanical properties and understand how they are affected.

The testing was conducted on the CellScale BioTester machine (CellScale, Waterloo, Ontario, Canada) to differentiate and understand the viscoelastic and failure properties of the AF. The AF samples will be tested at three different strain rates and will then be subjected to a failure test in tensile and shear directions. In future, the results from this study, which are stiffness and hysteresis loss coefficient, will provide data for the development of computational models for contributing to the diagnostic and therapeutic field for the management of lower back pain by analysing the relationship between the AF and its mechanical properties, and this will result in better decisions for treating patients and diagnostic outcomes.

LITERATURE REVIEW

Anatomy and Structure of the Disc

In the spine, we have a total of 25 intervertebral discs (IVDs) present between every two vertebrae (Nedresky et al., 2021). IVDs are fibrocartilage structures that exhibit degeneration with age and chronic illnesses, including diabetes and liver related problems, and are one of the main reasons for back pain (Adams and Dolan, 2012). The three main components of the IVD are the nucleus pulposus (NP), annulus fibrosus (AF), and cartilaginous endplates (CEP). AF is the fibre-reinforced layer, which is the outer layer that wraps and surrounds the inner NP, and the CEP encloses the inner NP from the top and bottom (Raj, 2008). NP is the inner or central region of the IVD; it has the consistency of a gelatinous structure. NP is important for the spine's flexibility and strength (Nedresky et al., 2021; Bayliss and Johnstone, 1992). In an adult IVD, NP makes up close to 50% of the total volume (Pooni et al., 1986). The caudal and cranial ends of the IVD are covered in thin hyaline cartilage layers, which are called the CEP, and their main function is to supply nutrients to the disc (Bae et al., 2013). CEPs are thinner towards the inside of the IVD (Vernon-Roberts and Pirie, 1977). Collectively, these three components of the IVD provide the functionality of the disc.

Figure removed due to copyright restriction

Figure 1: The internal structure of human IVD (Inoue, 1981)

Internal Structure of the Annulus Fibrosus

The AF is a fibre-reinforced tissue surrounding the NP. The AF is the focus of this study, on which micromechanical testing will be conducted to find out how diabetes affects its micromechanical properties. It is the outer region of the IVD and is made up of layers of collagen fibres and proteins, referred to as lamellae (Marchand and Ahmed, 1990). There are around 15 – 20 concentric lamellar layers, and the fibres are in a slanting position at a 30° angle (Southern Oregon Neurosurgical and Spine Associates Article). The thickness of the lamellar layers increases from the outer to inner layers, i.e., in the range of 0.05–0.5

mm. In each lamella, the collagen fibres run in the opposite direction to the adjacent layer, which makes them extremely strong and flexible at the same time (Cassidy et al., 1989). Figure 2 shows a cross-sectional view of the AF and its internal structure.

Figure removed due to copyright restriction

Figure 2: Cross-sectional view of the AF (Newell et al., 2017)

For this study, it is very critical to identify the function of the two respective lamellae in detail to understand how diabetes will alter them by affecting their micromechanical properties. Since the AF has a proteoglycan-rich matrix that holds the collagen fibres (O'Connell et al., 2011), that allows the AF to provide support and help distribute the major and multidirectional forces and strains that the IVD experiences, because of which all the structural components of the AF undergo various types of forces, and as they distribute throughout the vertebral column, it in turn affects the kinematics of the entire spine (Notaridis et al., 2006).

Mechanical Properties of the Annulus Fibrosus

The IVD undergoes a combination of torsion, bending, and compression stresses on a daily basis. The arrangement of the lamellae, which are weakly interconnected, determines the efficiency of the disc in producing motion (Inoue and Takeda, 1975). The NP deforms when the IVD is loaded in compression, causing the intradiscal pressure created within the disc to push it outward onto the CEP and the AF, and when the AF is pushed outward, they are loaded in tension. Since the AF works in tension, it can distribute the loads between the vertebral bodies (Adams and Roughley, 2006). AF exhibits viscoelastic responses when under mechanical loading. The viscoelasticity comes from intermolecular friction, i.e., flow-independent, and frictional drag force through the tissue matrix of the interstitial fluid flow (Iatridis et al., 1999; Powell et al., 1986).

Fujita et al., 1997 reported the difference in the ultimate and yield stresses of healthy and moderately degenerated AF samples and concluded that the moderately degenerated samples had a 30% decrease in their yield and ultimate stresses when compared to the healthy samples, proving that the AF becomes weaker when the disc is degenerated (Fujita et al., 1997). Iatridis et al., 1999 conducted a study to investigate the shear properties of the

AF between healthy and degenerated AF samples under compressive loading (Iatridis et al., 1999). They reported that the dynamic shear modulus was in the range of 100 – 400 kPa, and the frequency and strain amplitude affected it, causing a higher shear modulus under higher strain rates and a lower shear modulus under larger strains.

Effect of Diabetes on the Mechanical Properties

Diabetes mellitus is a condition where there is an excess of glucose present in the body. There are different types, such as type I, type II, and gestational diabetes. Diabetes causes an acceleration in the accumulation of AGEs in the biological tissues, causing them to degenerate faster (Dilworth et al., 2021). Diabetes affects the properties of bone materials in human beings. It is said that about 50% of diabetes patients are diagnosed with disc degeneration in the long term (Jakoi et al., 2017; Liu et al., 2018).

Due to the accumulation of AGEs, there is premature disc degeneration (Allen et al., 2015). There has been extensive research work done in the past on how the AGEs affect the soft tissues of the musculoskeletal system. They looked into the IVDs, tendons, articular cartilages, etc., to see how their tissue mechanics have been altered by using animal models with induced diabetes such as the murine, ovine, bovine, and porcine models (Reddy et al., 2002; Svensson et al., 2018). The results of the studies conducted by Krishnamoorthy et al., 2018 and D'Erminio et al., 2020 reported that connective tissue mechanics were altered as a decrease in viscoelasticity was observed with an increase in stiffness, failure strength, and toughness (Krishnamoorthy et al., 2018; D'Erminio et al., 2020). Using diabetic animal models, research studies were conducted to evaluate and understand the joint-level disc mechanics by inducing glycation by feeding an AGE-rich diet to the specimens, or the other method was by inducing in vitro crosslinking, and it was reported that there was increased joint stability and stiffness. Therefore, in vitro testing using non-enzymatic cross-linking glycation resulted in improved mechanical properties compared to in vivo testing (Hedman et al., 2006; Barbir et al., 2010; Kirking et al., 2013; Fields et al., 2015; Krishnomoorthy et al., 2018).

There is not much done on how the micromechanical properties of the AF are affected because of diabetes. There were two research studies conducted by the same group that focused on how diabetes affects the mechanical properties of the AF, conducted by Werbner et al., 2022 and Zhou et al., 2023, and the second study was a continuation of the first study. These studies used bovine samples and in vitro glycation techniques, which helped them to control the tissue hydration, as the main issue faced by past studies was excessive tissue

hydration (Han et al., 2012; Werbner et al., 2022). The first study was tested in the circumferential-axial direction at two loading rates, and the results reported that at the higher loading rate, the failure stress and modulus increased. The stiffness of the tissue increased as the loading rate also increased (Werbner et al., 2022). However, this was contrary to the past research studies conducted on tendons (Snedeker et al., 2012; Verzijl et al., 2002; Gautieri et al., 2017).

The main limitation of this study was that they only tested in the circumferential-axial direction, but in their subsequent study by Zhou et al., 2023, they tested in the circumferential-radial and radial directions, and the results showed that when the AGE content was increased, the radial failure stress increased by 40% and the tensile modulus by ~55% (Zhou et al., 2023). This study was a great advancement in the research field on how diabetes affects AF mechanical properties.

Effect of Strain Rate on the Annulus Fibrosus

To understand the effect of strain rate on the AF, it must be tested at various strain rates. For that purpose as reported in the published literature (Tavakoli and Costi, 2018), two different types of dynamic tests are typically conducted, they are non-destructive dynamic test, which is the slow, medium, and fast tests, and it would give the measure of modulus and hysteresis loss coefficient, and destructive dynamic test, i.e., the failure test in which the specimen is loaded to failure, and it would tell us about the toughness and strength of the specimens. A study by Tavakoli and Costi, 2018 using the CellScale microtensile testing machine (CellScale, Waterloo, Ontario, Canada) used three different strain rates of 0.1% (slow test), 1% (medium test), and 10% (fast test), and the results showed an increase in stiffness when the strain rate increased for all the specimens taken from all the circumferential regions as they underwent compression loading, and this was because the strain rate values were from a wider range (Tavakoli and Costi, 2018). From this, it was understood and concluded that the IVDs do exhibit viscoelastic properties. During the failure test, the failure force found was significantly higher in tension compared to when the specimens were under shear loading. This study showed strain rate-dependent behaviour during dynamic loading.

Gap in the Literature

All the previous research works have been conducted on animal models by inducing glycation artificially, which is a time-consuming and challenging process. There is very little

research being conducted on the effects of diabetes on the AF, and to be specific, only two studies have been conducted at the micromechanical level in this area. Therefore, this research study will bridge the gap in the literature by performing micromechanical testing on human cadaver AF samples between diabetic and healthy specimen groups to understand how the properties are affected.

The main aim of this research study is to investigate the effects of diabetes on the micromechanical properties of the AF in the posterior lateral (PLT) region using human cadaver specimens and to understand that the results of the diabetic group will be compared to those of the control (healthy) group. The tests will be performed using the CellScale BioTester machine (CellScale, Waterloo, Ontario, Canada), and the specimen will be tested at three different strain rates and then subjected to a failure test in the tensile and shear direction.

METHODOLOGY

This study was conducted on human cadaver IVD samples provided by the Biomechanics and Implant Laboratory, Room 5.24, situated at Flinders University, Tonsley campus. The specimens used in the formal study were divided into two groups, control group (n = 3, healthy or non-diabetic) and the diabetic group (n = 3, from diabetic cadavers). One additional healthy disc was used for pilot testing. For all testing of human tissue, specimens were taken from the PLT region of the IVD (Table 1). All slicing was completed by hand. The methodology used in this study was adapted from Tavakoli and Costi, 2018 for preparing and gripping the sample, and for experimental testing.

Table 1: Specimen Information and Demographics

Specimen number	Test	Disc level	Gender	Age (in years)	Group
GL191447	Pilot	L2 – L3	Male	34	Healthy
GL1809052	Formal	L1 – L2	Male	74	Diabetic
GL1911447	Formal	L2 – L3	Male	74	Diabetic
GL1911471	Formal	T12 – L1	Female	83	Diabetic
GL1808864	Formal	T12 – L1	Male	73	Healthy
GL1911504	Formal	L2 – L3	Male	25	Healthy
GL1912463	Formal	T12 – L1	Female	96	Healthy

The testing was conducted in three different stages using the same methodology. The first stage was the practice testing, which was conducted on two sheep IVDs to learn how to isolate the IVD from the functional spinal unit (FSU) and acquire the required skills and detailed techniques. The second stage was the pilot testing, which was conducted on one

healthy human cadaver IVD to confirm the methodology by Tavakoli and Costi, 2018 on human samples and to validate that it was repeatable. Lastly, formal testing was conducted on six human cadaver IVDs, i.e., three per group. After every stage of testing, the data was checked for consistency and quality. This gave a consistent and repeated testing methodology for each specimen (Figure 3).
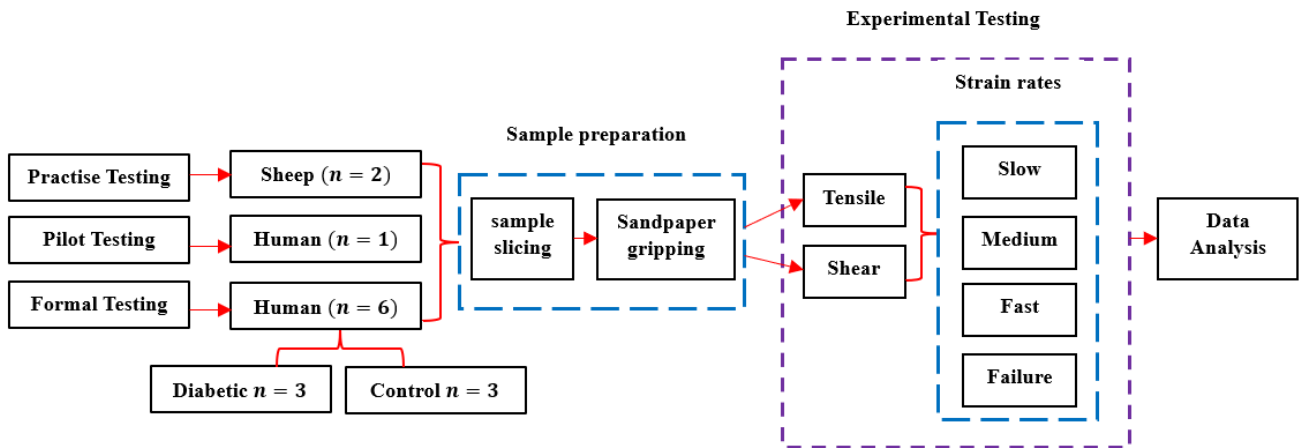

Figure 3: Flow diagram of the testing methodology

The disc isolation was practiced on sheep spines because of the limited availability of human samples. For pilot testing, the sheep discs ($n = 2$) were isolated from the whole FSU using a scalpel and bone cutter. It was noticed that the sheep disc was smaller in size and disc height, and the posterior region was lacking in thickness, due to which only the anterior and anterior lateral regions were tested (Appendix A, Figure 1).

Specimen Preparation

Human discs were isolated using the method derived from sheep disc isolation (Appendix B) and frozen at $-20°C$ and then they were taken out and immediately cut into $5\,mm$ wide segment blocks from the PLT region using a scalpel. The cuts were made exactly at a 90° angle downwards (Figure 4, a-b). Then a hand-held microtome was used for slicing segments by hand into $1\,mm$ thick slices. The microtome was adapted using a 3D-printed platform for holding the specimen and a circular rotating dial for moving the platform up and down (Appendix A, Figure 2).

The 3D-printed platform was lined with masking tape to create a mould and kept on the microtome (Figure 4, c). The $5\,mm$ wide PLT segment from the IVD was then placed in the mould and filled with optimal cutting temperature (OCT) compound (Tissue-Tek, Sakura,

Japan), and kept in the walk-in freezer at $-20°C$ for $50-55$ minutes to set the OCT (Figure 4, d). After, using a feather blade, two $1\ mm$ thick slices were cut transversely, by hand, and for measuring $1\ mm$ thickness the circular dial was turned two times clockwise with reference to zero on the scale on the hand-held microtome (Figure 4, e). Then phosphate-buffered saline (PBS) was sprayed to dissolve the OCT around the slices (Figure 4, f). Two slices of measurement $1\ mm\ (thickness) \times 5\ mm\ (width)$ were taken, one for tensile testing and one for shear tests. Since there were six specimens, in total, 12 slices were obtained. When one slice was getting prepared for testing, the other slice was wrapped in gauze and sprayed with PBS, then covered in cling wrap and kept back in the freezer. It is assumed that there is no damage to the AF tissue occurred while cutting and isolating it.
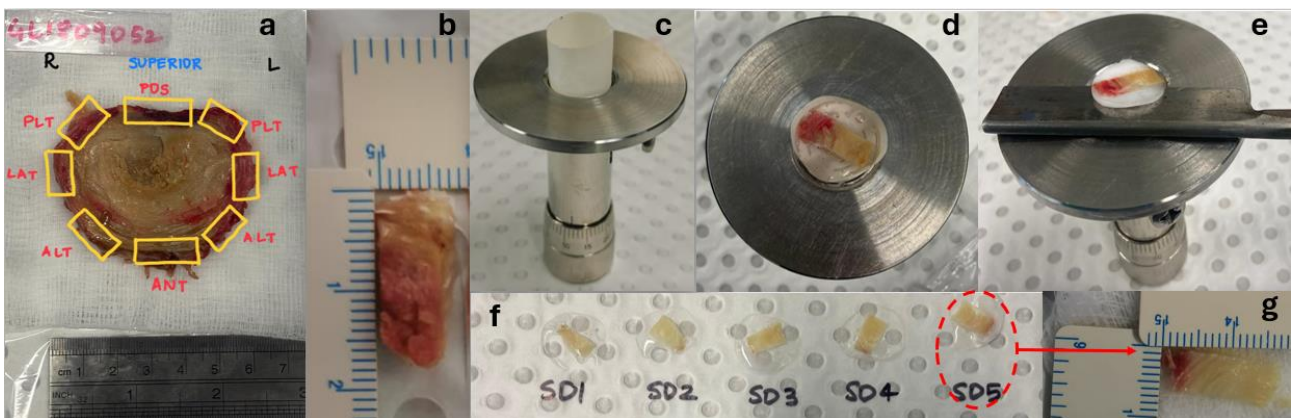

Figure 4: (a) Labelled human IVD, (b) 5 mm wide block cut, (c) masking tape mould for the microtome, (d) specimen with OCT compound, (e) cutting 1 mm transverse slice from the frozen sample, (f) Different slices obtained, (g) zoomed in picture of one slice

Gripping of the Specimen

The specimen slices of measurement $1\ mm\ (thickness) \times 5\ mm\ (width)$ (Figure 5, a) were gripped using sandpaper strips. These sandpaper strips were cut from 180 grit sandpaper sheets with a measurement of $7\ mm\ (width) \times 50\ mm\ (length)$ and then masking tape was wrapped on one end of the strips to help it float in the PBS bath while testing (Figure 5, b). The sliced specimen was placed on the rectangular glass slide, and using the microscope, two sets of functioning lamellae units consisting of two ILM were selected by looking for two pairs of one translucent layer (ILM) between two opaque layers (lamellae).

Loctite 480 back-dyed slow-setting glue was used for sticking the sandpaper strips to the specimen. A very small amount of glue was put on the strip and spread evenly using a thin needle (Figure 5, c). The excess glue was removed to avoid leakage. Then the strip was

very carefully stuck onto the specimen from the top and bottom so that the distant end of the slice was gripped. The first slice was prepared for tensile testing, and the second slice was prepared for shear testing (Figure 5, d-e). For shear testing, the specimen was placed 90° to its position in the tensile direction. After the glue was set (approximately 2 mins), the specimen was transferred to the testing CellScale BioTester (CellScale, Waterloo, Ontario, Canada) between two rectangular aluminium plates to keep its position intact.
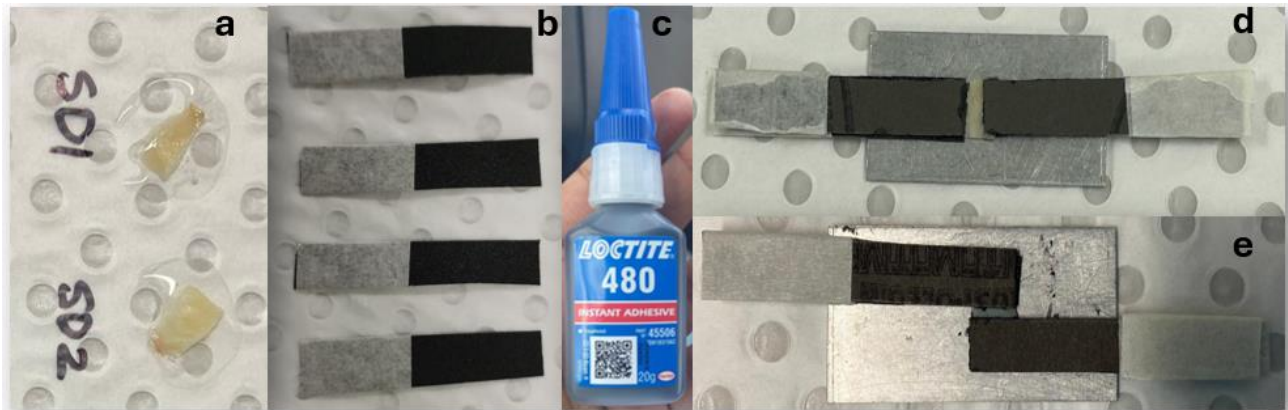

Figure 5: (a) Two slices of the specimens for testing, (b) sandpaper strips prepped using masking tape on one end, (c) Loctite 480 glue, (d) specimen prepared for tensile testing, (e) specimen prepared for shear testing

Experimental Testing

The prepared test specimen was released into the PBS bath of the CellScale machine, and then CellScale Labjoy software (CellScale, Waterloo, Ontario, Canada) was opened on the desktop, and the required template was selected. The PBS bath was lowered, and the prepared test specimen was released into the PBS bath of the CellScale BioTester machine (Figure 6, a), and then CellScale Labjoy software (CellScale, Waterloo, Ontario, Canada) was opened on the desktop and the required template was selected. The PBS bath was lowered, the actuators were reset, and then the distance from the gripper-to-gripper end was measured using a digital vernier calliper and entered into the system, and the actuators were moved to the measured distance, which was specimen specific. The specimen was then loaded onto the clamps of the device, and the lights were positioned correctly (Figure 6, b-c). After that, the microscope camera's contrast and focus were adjusted accordingly. Then a preload of 100 mN was applied to the specimen. The specimen was subjected to non-destructive dynamic tests at three different strain rates, which are slow ($0.1 \%s^{-1}$), medium ($1 \%s^{-1}$), and fast ($10 \%s^{-1}$), where the frequency for data acquisition was set at 1 Hz, 5 Hz, and 100 Hz, respectively. For each strain rate, five cycles of dynamic loading were performed, after which the specimen was subjected to the destructive test (failure test) at a

10% strain rate. All these tests were performed in tensile and shear loading directions. Here, it is assumed that the obtained data is consistent and accurate, and the calibration of the CellScale machine has been performed.
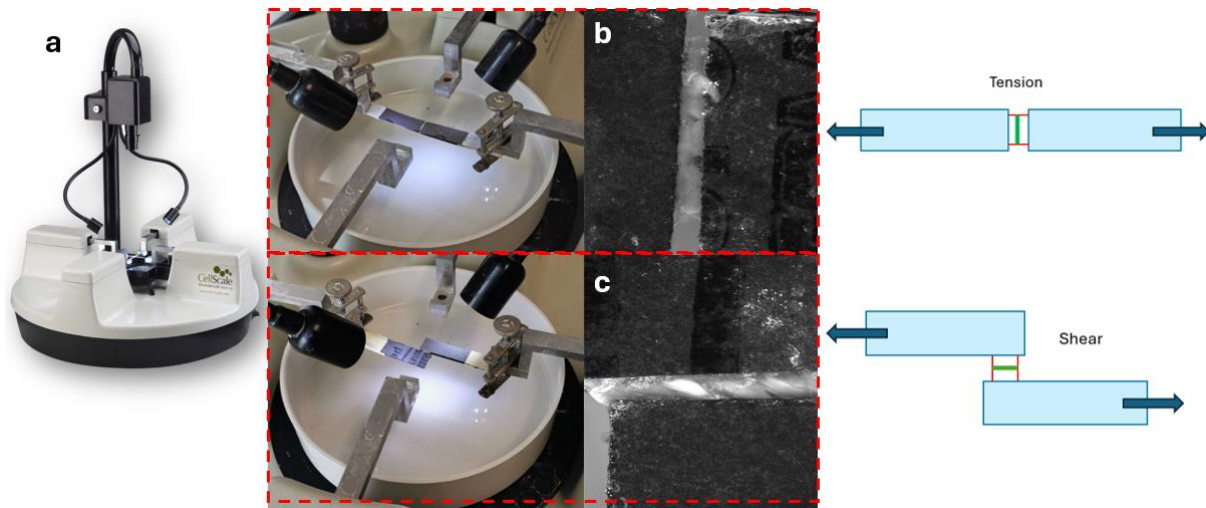

Figure 6: CellScale BioTester machine, (b) specimen loaded in the tensile direction, (c) specimen loaded in the shear direction

Data Analysis

By conducting the practice test on sheep and the pilot test on a human disc, the methodology was validated as the data obtained was consistent. Its repeatability was confirmed as the analysed data provided intended results, and it confirmed the mechanical properties, such as the viscoelasticity and failure load, of the IVD. Measures obtained from CellScale were force (mN), time (seconds), and displacement (μm) and using the MS Excel template, the force versus time and force versus displacement graphs were plotted. For the data analysis to provide acceptable results, the specimens and respective test results underwent quality check strategies such as making sure the dimensions of the specimen were uniform according to the given measurements in the protocol, ensuring there is no slippage of the specimen, to validate the gripping technique, the response of the sample to the testing should present optimal results, and that was confirmed from the force versus displacement graph, and there should not be leakage of glue over the specimen.

Then, by calculating the area of the gripped specimen using the width and thickness of the specimen, the stress was obtained from the ratio of the force and area. The strain was obtained as the ratio between the change in length and the initial length. This was then plotted using the MS Excel template. From the calculated stress and strain data of the last cycle, the stiffness was calculated by putting the best line of fit in the loading curve's linear

region and obtaining the slope using the linear regression formula. The linear region for the line of best fit was chosen between 25% and 35% of the last cycle's loading region (Tavakoli and Costi, 2018) then maximum stress was obtained. Also, the hysteresis loss coefficient was obtained from the area calculated using the stress and strain curves. The hysteresis loss coefficient is the area between the last cycle's loading and unloading curve and dividing it by the area under the loading curve using the trapezoid polynomial formula in the MS Excel template. For the failure test, force versus displacement graphs were plotted and using the MS Excel template the failure load or maximum force was acquired and energy absorbed was calculated. Due to the small sample size, the median and interquartile range (IQR) were calculated and represented using error bars on the graphs to determine the correlated variations in the data, instead of the mean and standard deviation. Results were analysed using the graphs plotted from the data directly on MS Excel, and these trends were then compared and discussed. For the formulas used for all the calculation refer Appendix C.

RESULTS

In the formal testing stage, two AF slices, from each of six specimens were tested in total, i.e., three specimens each from the control (healthy or non-diabetic) group and diabetic group. One of the two slices were tested in tension and the other slice in shear. Each slice was subjected to non-destructive tests at three strain rates, followed by a destructive (failure) test, representing a total of four tests per specimen. Therefore, in total, 48 tests were conducted to obtain the results for this study. It was confirmed that the sandpaper with glue gripping technique showed no slippage since no relative motion between the sandpaper and specimen was observed throughout the testing. Hence, no tests were excluded from the results.

Briefly, all methods were first piloted using sheep IVD to reinforce good technique and repeatable testing. Upon completion of the pilot testing, the specimens were repeatedly showed no slippage and consistent loading curves (Appendix A, Figure 3). All the results were first tabulated, compared and then plotted (Appendix D).

Non-Destructive Testing

Maximum Stress

The median $\pm$ IQR values of the maximum stress at three different strain rates ($0.1\ \%s^{-1}, 1\ \%s^{-1}, and\ 10\ \%s^{-1}$) were calculated for three specimens at each strain per group between tensile and shear tests for the control and diabetic groups. Generally,

diabetic specimens appeared stiffer in the tension direction across all loading rates (Figure 7).

Figure 7: Median maximum stress at different strain rates

Stiffness

The median $\pm$ IQR values of the stiffness at three different strain rates $(0.1\ \%s^{-1}, 1\ \%s^{-1}, and\ 10\ \%s^{-1})$ were calculated for three specimens at each strain per group between tensile and shear tests for the control and diabetic groups. Generally, diabetic specimens appeared stiffer in the tension direction across all loading rates (Figure 8).
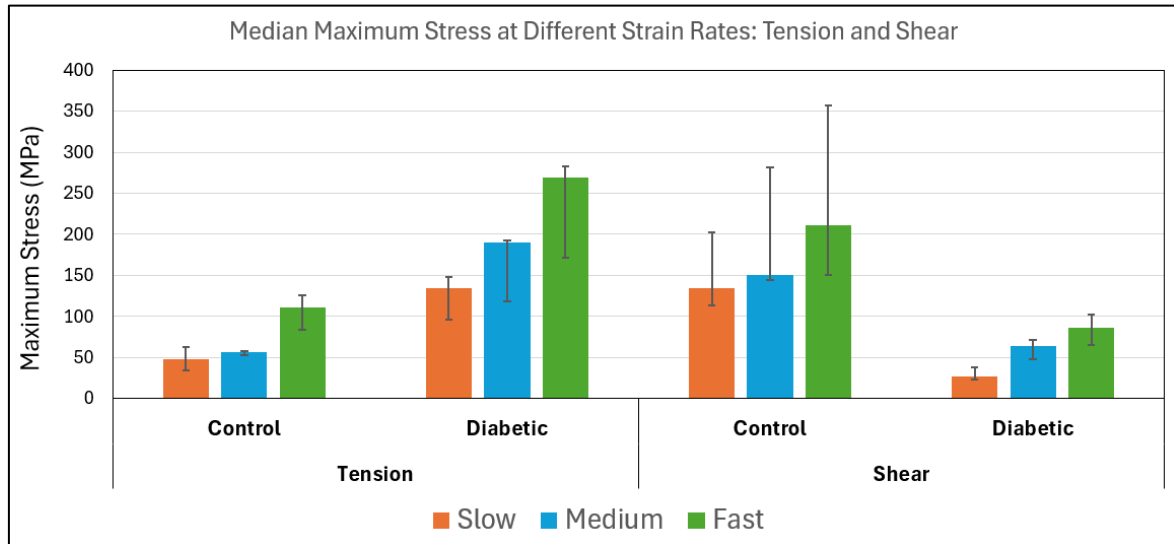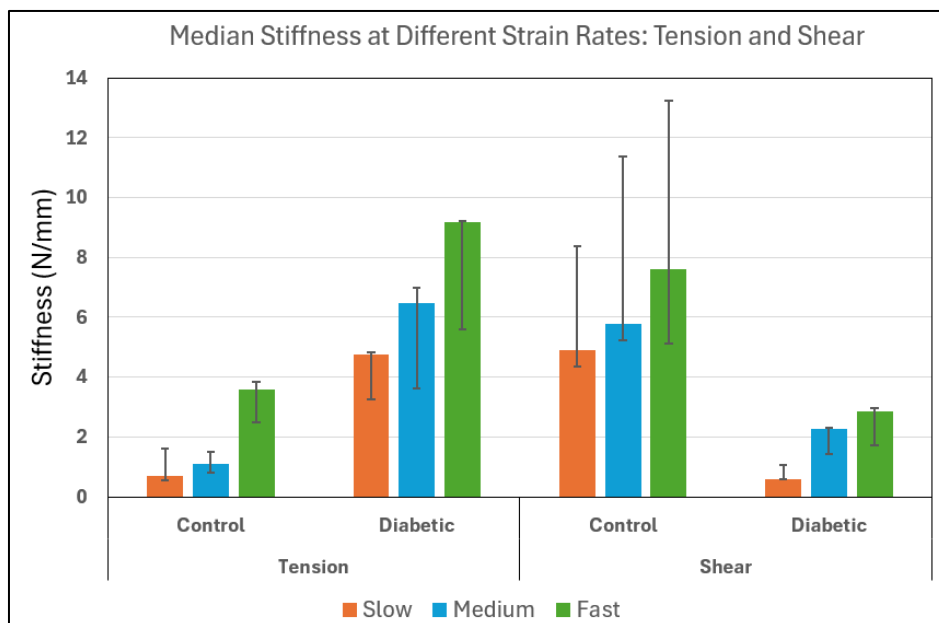

Figure 8: Median stiffness at different strain rates

Hysteresis Loss Coefficient

The median $\pm$ IQR values of the hysteresis loss coefficient at three different strain rates ($0.1\,\%s^{-1}, 1\,\%s^{-1}, and\,10\,\%s^{-1}$) were calculated for three specimens at each strain per group between tensile and shear tests for the control and diabetic groups (Figure 9). This was obtained by dividing the energy absorbed by the area under the loading curve. In the graph given below, the x-axis represents the different tests, and the y-axis represents the hysteresis loss coefficient.
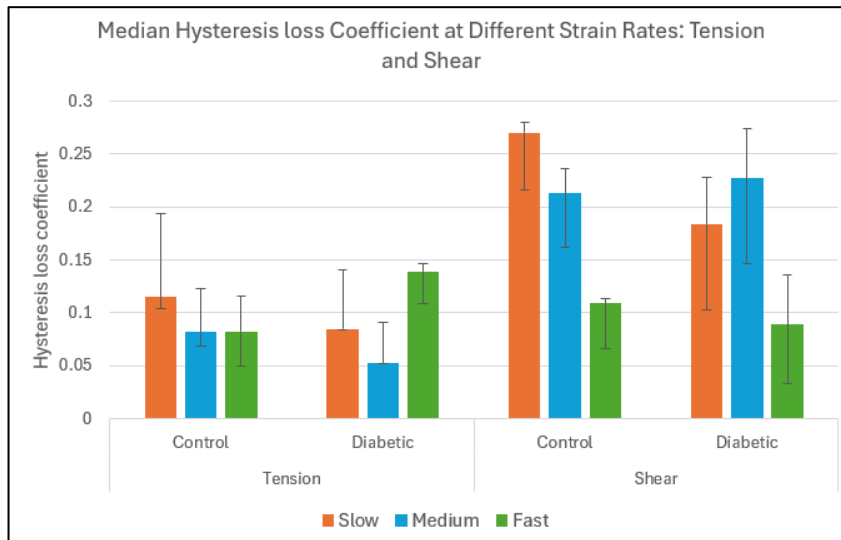
Figure 9: Median hysteresis loss coefficient at different strain rates

Destructive or Failure Testing

Destructive testing was conducted under tensile and shear directions for every specimen. The specimen was subjected to a ramp test to failure at a strain rate of $10\,\%s^{-1}$ and the median $\pm$ IQR values of the peak force and the energy absorbed at failure were calculated.
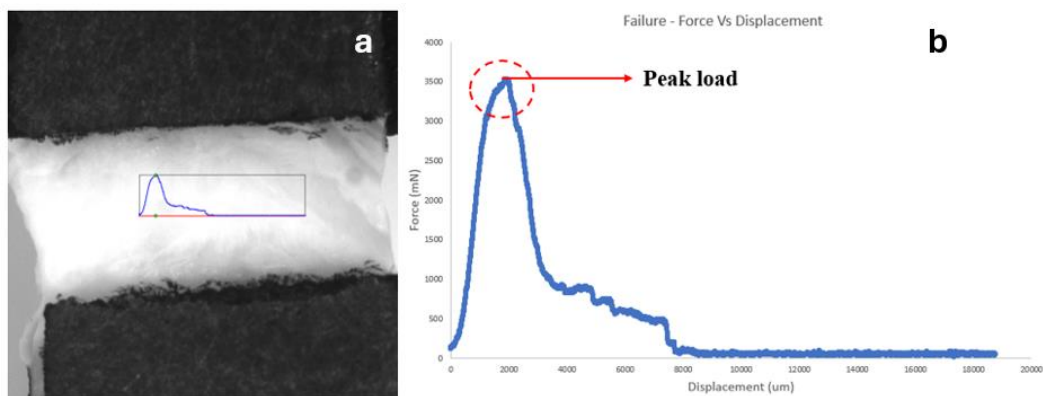
Figure 10: (a) Specimen at peak failure load, (b) Graph representing the failure test

Figure 10 indicates the peak force at which the specimen starts to tear in the tensile direction from the load applied.

Failure Load

The median ± IQR values of the peak load at failure were calculated for three specimens per group between tensile and shear tests for the control and diabetic groups. Generally, the peak force at failure is less for diabetic specimens in the shear direction (Figure 11).

Figure 11: Median peak load at failure at different strain rates

Energy Absorbed at Failure

Figure 12: Median energy absorbed at failure at different strain rates

The median $\pm$ IQR values of the energy absorbed at failure were calculated for three specimens per group between tensile and shear tests for the control and diabetic groups. Generally, the peak force at failure is less for diab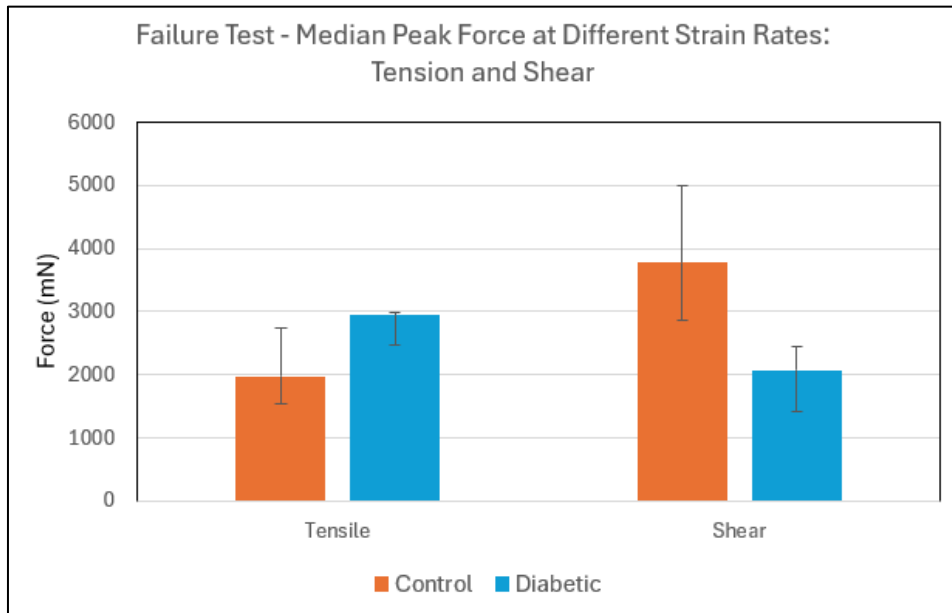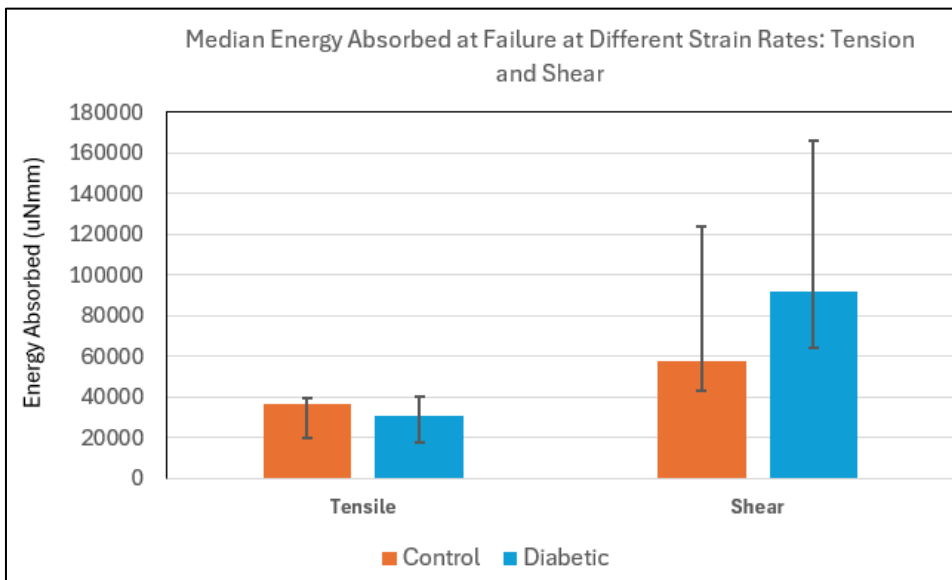etic specimens in the shear direction (Figure 12). The energy absorbed is the area under the loading and unloading curve.

DISCUSSION

All the graphs are plotted from the final cycle of the testings, and all the mechanical properties examined for the control and diabetic groups exhibited viscoelastic behaviour. The data analysis of the obtained data showed distinguishable trends, of which some were consistent with the past literature, and some were inconsistent. The results are discussed and compared in detail in the sections below.

Non-Destructive Testing - Viscoelasticity
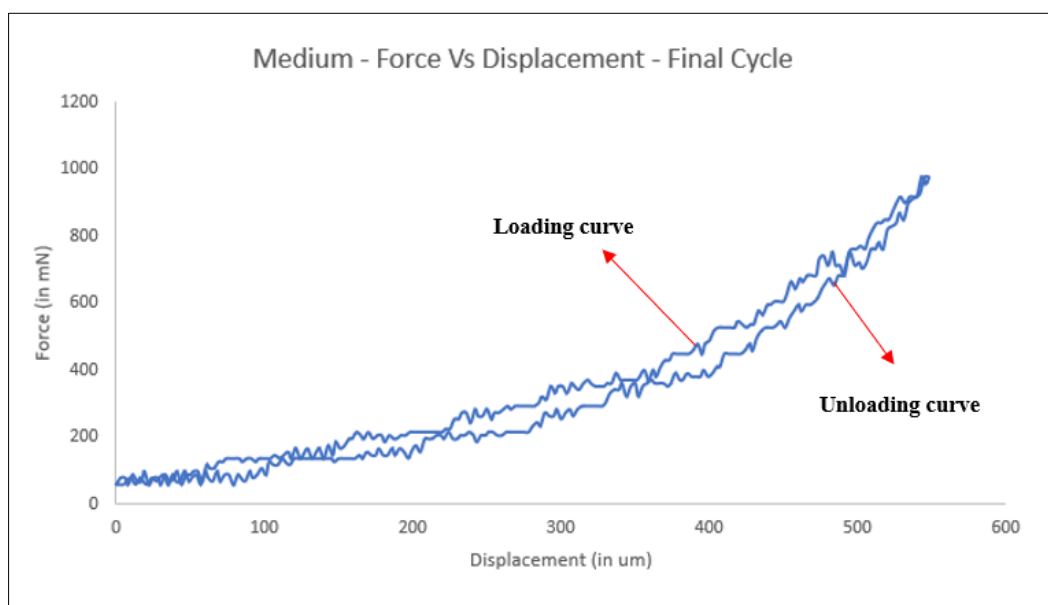
Figure 13: Graph showing the loading and unloading curves of the final cycle

The stress versus strain and force versus displacement curves of the non-destructive testing conducted on the specimens showed viscoelastic behaviour (Figure 13). The loading and unloading curves demonstrate that the specimen underwent displacement when the force was applied during the loading phase but returned to its original position during the unloading phase. This representation also shows hysteresis loss, i.e., the area under the loading and unloading curves, which is expected from the mechanical properties of soft tissues. The specimens had a strain-rate response, which means that differing energies and

stiffnesses were observed across the three different strain rates, i.e., the specimen stiffens as the strain rate got faster, more like a solid. The stress versus strain graph shows the final loading of the same specimen at the three different strain rates for tensile testing, and it shows how stiffness increases with the increasing loading rate (Appendix A, Figure 3).

Stiffness

The stiffness was seen to increase with the increasing strain rate in both the tensile and shear directions in both groups of specimens, i.e., the specimen was starting to act like a solid as the strain rate increased. It was noticed that in the tensile direction, the diabetic specimens were comparatively stiffer than the healthy specimens. This finding is in agreement with the results of the previous study conducted by Krishnamoorthy et al., 2008 and D'Erminio et al., 2020 on the diabetic animal model. Which stated that stiffness increases when affected by diabetes (Krishnamoorthy et al., 2008 and D'Erminio et al., 2020). However, in the shear direction, it was contracting these results as the diabetic specimens had lower stiffness, this could be because shear is also naturally weaker, similar to Tavakoli and Costi, 2018, where they stated that shear has a low modulus (Tavakoli and Costi, 2018).

The loosening of the tissue fibres in the testing sample was noticed while loading the sample after the slow test in the shear direction for two specimens, where the specimen looked stretched in the video recordings of these tests. There was an issue with the preload, as it was noticed that it was not reaching 100 mN as quickly as it was supposed. This could be due to the stretched tissue fibres, because of which the machine was not able to apply the required force. This also led to testing the same slice of specimen twice at a medium strain rate and twice at a fast strain rate for specimen GL1809052. For GL1911471, it was tested twice at a medium strain rate, and both of these situations occurred during shear testing. However, the reason for the loosening of the tissue fibres is not known.

Maximum Stress

The maximum stress increased with the increasing strain rate and in the tensile direction. It was shown that the diabetic specimens had higher maximum stress compared to the control group, maybe because they are stiffer compared to the healthy specimens. However, in the shear direction, it was the opposite, and the reason could be the same as mentioned for stiffness, the loosening of the tissue fibres while testing.

Hysteresis Loss Coefficient

The hysteresis loss coefficient was observed to be high at a slow strain rate and reduced when the strain rate was increased, but this trend was only seen in the control specimen group. The diabetic group had variance in their hysteresis loss coefficient levels. This hysteresis loss coefficient gave an indicator of how much energy is absorbed through the whole cycle, i.e., the loading and unloading phases.

The overall trend of the graph showed that the hysteresis loss coefficient is considerably less in the tensile direction compared to the control group; however, in the shear direction, it was only slightly less. The hysteresis loss coefficient was highest in the shear direction for the slow strain rate for the control group, and the lowest was in the tensile direction for the diabetic group for the medium strain rate. For the specimen GL1809052, the hysteresis loss coefficient was -0.0229 which was contradictory as this means there was energy gain instead of loss, and this could be possibly due to the sandpaper giving a spring effect on the specimen. However, it was not possible to exclude this result from the calculation because of the small sample size. Overall, the specimens taken for this study exhibited viscoelastic properties with their strain rate-dependent behaviour and hysteresis.

Failure Load

This is the peak load that is recorded during the failure test. During the failure test, the first of point deformation is at yield strength, and when the force becomes greater than yield strength, it reaches the peak load or maximum force. This is the second point of deformation, or the plastic region, where the specimen will break, leading to permanent deformation.

The peak load at failure was high for the diabetic group compared to the control group in the tensile direction, but this trend contradicts the results of the study done by Werbner et al., 2022, which say that diabetes leads to a decrease in failure load as the tissues are stiffer in nature, which leads to failure faster, but this variation could be because of difference in the testing method. However, in the shear direction, the results are consistent with the previous literature, where the diabetic group shows less peak load at failure compared to the control specimen because the healthy specimens have a higher peak load at failure. It also has to be considered that the study conducted by Werbner et al., 2022 was tested on bovine samples in the anterior and posterior regions only at two loading rates (high and low). The contradiction in the results could be because of this reason (Werbner et al., 2022).

Energy Absorbed at Failure

The energy absorbed at failure was calculated for control and diabetic specimens between tensile and shear tests, and their median and IQR values were obtained. The graph showed that the energy absorbed was less compared to the control group in the tensile direction, and it was the opposite in the shear direction. In the tensile direction, the median ± IQR values between the control and diabetic groups did not have too much variance and were close to constant. However, in the shear direction, the diabetic specimens had a higher value compared to the control group.

Limitations

The main aim of this research study was to investigate the effects of diabetes on the micromechanical properties, such as stiffness, viscoelasticity, hysteresis loss coefficient, and failure load of the AF in the PLT region using human cadaver specimens, and that was achieved successfully. However, this study has a few limitations that must be addressed. The first one being the sample size; it was n = 3 for the control and diabetic groups, respectively, and for this study, and that was a small sample size, which did not provide sufficient data for statistical analysis. Also, because of a few issues with slicing the specimen using the hand-held microtome, there were tears in the initial slices, due to which they could not be used. This reduced the number of slices from the specimens, because of which repeatability testing was not possible if time permitted. Due to the small sample size, there was variability among the data obtained from the specimens because of which comparing the results to previous literature was challenging.

Due to the limited availability of human IVD samples, the specimens were not from the same age group, and the genders of the specimens were also different. Because of these factors, a proper comparison could not be carried out between different age groups and both genders, as there was not enough data to do this. The next limitation is the IVDs being from mixed vertebrae levels instead of from the same level, this again being due to the difficulty in finding human specimens. This factor could have led to a few variations in the results, as there could be differences in the mechanical properties between different vertebrae levels, even though it is not a big difference. There was no control over the diabetic history of the specimens, because of which it was not known for how long they have had diabetes. However, it was mentioned in the donor summary that one of the specimens had type II diabetes, and for the other two specimens, it just said history of diabetes. Having this information could help a lot in interpreting the results and having a better understanding.

CONCLUSION

In conclusion, the main purpose of this research study was to look into how diabetes affects the micromechanical properties of the AF in the PLT region. This was achieved by examining the AF from human cadaver samples and obtaining results in terms of viscoelasticity, and the stiffness, maximum stress, hysteresis loss coefficient, and failure load and energy absorbed at failure were calculated from the data obtained in terms of time, force, and displacement. The effects of diabetes on these micromechanical properties at three different strain rates at tensile and shear loading directions were obtained and compared between healthy and diabetic specimen groups using the methodology adapted from the study by Tavakoli and Costi, 2018. The findings of this study are that the diabetic specimens showed higher stiffness compared to the healthy specimens in the tensile direction, but in the shear direction it showed lower stiffness. Hysteresis loss coefficient was considerably lower in the tensile direction; and the diabetic specimens showed lower failure load in the shear direction. Along the way, a few limitations were experienced, due to which there was variability in some of the results. There was no control over the diabetic history, age, and gender of the specimens and from which vertebral level the discs were harvested. The biggest limitation was the small sample size. The data and results obtained from this study are a significant step closer towards to understanding the effects of diabetes on the AF, as there is very little study done in that research area and adding to the database of mechanical properties will contribute to combining experimental side with computational techniques to improve the methods for diagnostics in future.

FUTURE WORKS

For the future extension of this research study, instead of human cadaver AF samples, testing can be conducted on surgically retrieved human AF samples, and then the specimens of the study can be categorised based on their diabetic history, age, and gender. And then the results can be compared to see how they affect different categories. The study could also use a larger sample size from which sufficient data can be obtained to conduct statistical analysis using IBM SPSS to perform the ANOVA test. To have a better understanding of the tissue creep and stress relaxation tests can be conducted. Furthermore, the regions can be divided into outer and inner regions for further categorization. Overall, a larger sample size and control over the various factors mentioned above will provide a better understanding of the effects of diabetes on the AF.

BIBLIOGRAPHY

Adams, M.A. and Dolan, P. (2012). Intervertebral disc degeneration: evidence for two distinct phenotypes. Journal of Anatomy, 221(6), pp.497–506. doi:https://doi.org/10.1111/j.1469-7580.2012.01551.x

Adams, M.A. and Roughley, P.J. (2006). What is Intervertebral Disc Degeneration, and What Causes It? Spine, 31(18), pp.2151–2161. doi:https://doi.org/10.1097/01.brs.0000231761.73859.2c.

Allen, M.R., Newman, C.L., Chen, N., Granke, M., Nyman, J.S. and Moe, S.M. (2015). Changes in skeletal collagen cross-links and matrix hydration in high- and low-turnover chronic kidney disease. Osteoporosis international: a journal established as result of cooperation between the European Foundation for Osteoporosis and the National Osteoporosis Foundation of the USA, [online] 26(3), pp.977–985. doi:https://doi.org/10.1007/s00198-014-2978-9.

Bae, W.C., Statum, S., Zhang, Z., Yamaguchi, T., Wolfson, T., Gamst, A.C., Du, J., Bydder, G.M., Masuda, K. and Chung, C.B. (2013). Morphology of the Cartilaginous Endplates in Human Intervertebral Disks with Ultrashort Echo Time MR Imaging. Radiology, [online] 266(2), pp.564–574. doi:https://doi.org/10.1148/radiol.12121181.

Barbir, A., Michalek, A.J., Abbott, R.D. and Iatridis, J.C. (2010). Effects of enzymatic digestion on compressive properties of rat intervertebral discs. Journal of Biomechanics, 43(6), pp.1067–1073. doi:https://doi.org/10.1016/j.jbiomech.2009.12.005.

Bayliss, M., Johnstone, B., 1992. Biochemistry of the intervertebral disc. In: Jayson, M.I.V., Dixon, A.S.J.

(Eds.), The Lumbar Spine and Back Pain. Churchill Livingstone, Edinburgh, 111–131.

Bloom, D., Boersch-Supan, A., Mcgee, P. and Seike, A. (2011). PROGRAM ON THE GLOBAL DEMOGRAPHY OF AGING Population Aging: Facts, Challenges, and Responses Population Aging: Facts, Challenges, and Responses. [online] Available at: https://www.hsph.harvard.edu/wp-content/uploads/sites/1288/2013/10/PGDA_WP_71.pdf.

Buckwalter, J.A. (1995). Aging and degeneration of the human intervertebral disc. Spine, [online] 20(11), pp.1307–14. doi:https://doi.org/10.1097/00007632-199506000-00022.

Cassidy, J.J., Hiltner, A. and Baer, E. (1989). Hierarchical Structure of the Intervertebral Disc. Connective Tissue Research, 23(1), pp.75–88. doi:https://doi.org/10.3109/03008208909103905.

Castro, A.L., Ribeiro-Machado, C., Oliveira, C.M., Teixeira, G.Q., Neidlinger-Wilke, C., Pereira, P., Vaz, R., Barbosa, M.A. and Gonçalves, R.M. (2022). Fibrotic alterations in human annulus fibrosus correlate with progression of intervertebral disc herniation. Arthritis Research & Therapy, 24(1). doi:https://doi.org/10.1186/s13075-021-02690-w.

Chan, S.C.W., Ferguson, S.J. and Gantenbein-Ritter, B. (2011). The effects of dynamic loading on the intervertebral disc. European Spine Journal, [online] 20(11), pp.1796–1812. doi:https://doi.org/10.1007/s00586-011-1827-1.

Dilworth, L., Facey, A. and Omoruyi, F. (2021). Diabetes Mellitus and Its Metabolic Complications: The Role of Adipose Tissues. International Journal of Molecular Sciences, 22(14), p.7644. doi:https://doi.org/10.3390/ijms22147644.

Fields, A.J., Berg-Johansen, B., Metz, L.N., Miller, S., La, B., Liebenberg, E.C., Coughlin, D.G., Graham, J.L., Stanhope, K.L., Havel, P.J. and Lotz, J.C. (2015). Alterations in intervertebral disc composition, matrix homeostasis and biomechanical behavior in the UCD-T2DM rat model of type 2 diabetes. Journal of orthopaedic research : official publication of the Orthopaedic Research Society, [online] 33(5), pp.738–746. doi:https://doi.org/10.1002/jor.22807.

Fujita, Y., Duncan, N.A. and Lotz, J.C. (1997). Radial tensile properties of the lumbar annulus fibrosus are site and degeneration dependent. Journal of Orthopaedic Research, 15(6), pp.814–819. doi:https://doi.org/10.1002/jor.1100150605.

Gautieri, A., Passini, F.S., Silván, U., Guizar-Sicairos, M., Carimati, G., Volpi, P., Moretti, M., Schoenhuber, H., Redaelli, A., Berli, M. and Snedeker, J.G. (2017). Advanced glycation end-products: Mechanics of aged collagen from molecule to tissue. Matrix Biology, 59, pp.95–108. doi:https://doi.org/10.1016/j.matbio.2016.09.001.

Han, W.M., Nerurkar, N.L., Smith, L.J., Jacobs, N.T., Mauck, R.L. and Elliott, D.M. (2012). Multi-scale Structural and Tensile Mechanical Response of Annulus Fibrosus to Osmotic Loading. Annals of Biomedical Engineering, 40(7), pp.1610–1621. doi:https://doi.org/10.1007/s10439-012-0525-4.

Hedman, T.P., Saito, H., Vo, C. and Chuang, S.-Y. (2006). Exogenous cross-linking increases the stability of spinal motion segments. Spine, [online] 31(15), pp.E480-485. doi:https://doi.org/10.1097/01.brs.0000224531.49174.ea.

Hoy, R.C., D'Erminio, D.N., Krishnamoorthy, D., Natelson, D.M., Laudier, D.M., Illien-Jünger, S. and Iatridis, J.C. (2020). Advanced glycation end products cause RAGE-dependent annulus fibrosus collagen disruption and loss identified using in situ second harmonic generation imaging in mice intervertebral disk in vivo and in organ culture models. JOR spine, [online] 3(4), p.e1126. doi:https://doi.org/10.1002/jsp2.1126.

Iatridis, J.C., Kumar, S., Foster, R.J., Weidenbaum, M. and Mow, V.C. (1999). Shear mechanical properties of human lumbar annulus fibrosus. Journal of Orthopaedic Research: Official Publication of the Orthopaedic Research Society, [online] 17(5), pp.732–737. doi:https://doi.org/10.1002/jor.1100170517.

Inoue, H. and Takeda, T. (1975). Three-Dimensional Observation of Collagen Framework of Lumbar Intervertebral Discs. Acta Orthopaedica Scandinavica, 46(6), pp.949–956. doi:https://doi.org/10.3109/17453677508989283.

International Diabetes Federation (2021). IDF Diabetes Atlas 10th edition 2021. [online] IDF Diabetes Atlas. Available at: https://diabetesatlas.org/.

Jakoi, A.M., Pannu, G., D'Oro, A., Buser, Z., Pham, M.H., Patel, N.N., Hsieh, P.C., Liu, J.C., Acosta, F.L., Hah, R. and Wang, J.C. (2017). The Clinical Correlations between Diabetes, Cigarette Smoking and Obesity on Intervertebral Degenerative Disc Disease of the Lumbar Spine. Asian Spine Journal, 11(3), p.337. doi:https://doi.org/10.4184/asj.2017.11.3.337.

Jhawar, B.S., Fuchs, C.S., Colditz, G.A. and Stampfer, M.J. (2006). Cardiovascular risk factors for physician-diagnosed lumbar disc herniation. The Spine Journal, 6(6), pp.684–691. doi:https://doi.org/10.1016/j.spinee.2006.04.016.

Kirking, B.C., Toungate, J.K. and Hedman, T.P. (2013). The dose response relationship between intervertebral disc flexion-extension neutral zone metrics and injected genipin concentration. Journal of Applied Biomaterials & Functional Materials, [online] 11(2), pp.e73-79. doi:https://doi.org/10.5301/JABFM.5000151.

Krishnamoorthy, D., Hoy, R.C., Natelson, D.M., Torre, O.M., Laudier, D.M., Iatridis, J.C. and Illien-Jünger, S. (2018). Dietary advanced glycation end-product consumption leads to mechanical stiffening of murine intervertebral discs. Disease Models & Mechanisms, 11(12), p.dmm036012. doi:https://doi.org/10.1242/dmm.036012.

Lintz, M., Walk, R.E., Tang, S.Y. and Bonassar, L.J. (2022). The degenerative impact of hyperglycemia on the structure and mechanics of developing murine intervertebral discs. JOR spine, 5(1). doi:https://doi.org/10.1002/jsp2.1191.

Liu, X., Pan, F., Ba, Z., Wang, S. and Wu, D. (2018). The potential effect of type 2 diabetes mellitus on lumbar disc degeneration: a retrospective single-center study. Journal of Orthopaedic Surgery and Research, 13(1). doi:https://doi.org/10.1186/s13018-018-0755-8.

Luoma, K., Riihimäki, H., Luukkonen, R., Raininko, R., Viikari-Juntura, E. and Lamminen, A. (2000). Low Back Pain in Relation to Lumbar Disc Degeneration. Spine, 25(4), pp.487–492. doi:https://doi.org/10.1097/00007632-200002150-00016.

Mäntyselkä, P., Miettola, J., Niskanen, L. and Kumpusalo, E. (2008). Chronic pain, impaired glucose tolerance and diabetes: A community-based study. Pain, 137(1), pp.34–40. doi:https://doi.org/10.1016/j.pain.2007.08.007.

MARCHAND, F. and AHMED, A.M. (1990). Investigation of the Laminate Structure of Lumbar Disc Anulus Fibrosus. Spine, 15(5), pp.402–410. doi:https://doi.org/10.1097/00007632-199005000-00011.

Nedresky, D., Reddy, V. and Singh, G. (2021). Anatomy, Back, Nucleus Pulposus. [online] PubMed. Available at: https://www.ncbi.nlm.nih.gov/books/NBK535373/.

Notaridis, G., Ebbing, K., Giannakopoulos, P., Bouras, C. and Kovari, E. (2006). Neuropathological analysis of an asymptomatic adult case with Dandy-Walker variant. Neuropathology and Applied Neurobiology, 32(3), pp.344–350. doi:https://doi.org/10.1111/j.1365-2990.2006.00719.x.

O'Connell, G.D., Sen, S. and Elliott, D.M. (2011). Human annulus fibrosus material properties from biaxial testing and constitutive modeling are altered with degeneration. Biomechanics and Modeling in Mechanobiology, 11(3-4), pp.493–503. doi:https://doi.org/10.1007/s10237-011-0328-9.

Pooni, J., Hukins, D., Harris, P., Hilton, R. and Davies, K. (1986). Comparison of the structure of human intervertebral discs in the cervical, thoracic and lumbar regions of the spine. Surgical and Radiologic Anatomy, 8(3), pp.175–182. doi:https://doi.org/10.1007/bf02427846.

Powell, M.C., Szypryt, P., Wilson, M., Symonds, E.M. and Worthington, B.S. (1986). PREVALENCE OF LUMBAR DISC DEGENERATION OBSERVED BY MAGNETIC RESONANCE IN SYMPTOMLESS WOMEN. The Lancet, 328(8520), pp.1366–1367. doi:https://doi.org/10.1016/s0140-6736(86)92008-8.

Raj, P.P. (2008). Intervertebral Disc: Anatomy-Physiology-Pathophysiology-Treatment. Pain Practice, [online] 8(1), pp.18–44. doi:https://doi.org/10.1111/j.1533-2500.2007.00171.x.

Reddy, G.Kesava., Stehno-Bittel, L. and Enwemeka, C.S. (2002). Glycation-Induced Matrix Stability in the Rabbit Achilles Tendon. Archives of Biochemistry and Biophysics, 399(2), pp.174–180. doi:https://doi.org/10.1006/abbi.2001.2747.

Sapra, A. and Bhandari, P. (2022). Diabetes Mellitus. [online] PubMed. Available at: https://www.ncbi.nlm.nih.gov/books/NBK551501/#:~:text=Diabetes%20mellitus%20(DM)%20is%20a%20metabolic%20disease%2C%20involving%20inappropriately.

Snedeker, J.G. and Gautieri, A. (2014). The role of collagen crosslinks in ageing and diabetes - the good, the bad, and the ugly. Muscles, Ligaments and Tendons Journal, [online] 4(3), pp.303–308. Available at: https://pubmed.ncbi.nlm.nih.gov/25489547/ [Accessed 20 Oct. 2023].

Svensson, R.B., Smith, S.T., Moyer, P.J. and Magnusson, S.P. (2018). Effects of maturation and advanced glycation on tensile mechanics of collagen fibrils from rat tail and Achilles tendons. Acta Biomaterialia, 70, pp.270–280. doi:https://doi.org/10.1016/j.actbio.2018.02.005.

Takahashi, S., Suzuki, A., Toyoda, H., Terai, H., Sho Dohzono, Yamada, K., Matsumoto, T., Yasuda, H., Tsukiyama, K., Shinohara, Y., Ibrahim, M. and Nakamura, H. (2013). Characteristics of Diabetes Associated With Poor Improvements in Clinical Outcomes After Lumbar Spine Surgery. 38(6), pp.516–522. doi:https://doi.org/10.1097/brs.0b013e318273583a.

Tavakoli, J. and Costi, J.J. (2018). New insights into the viscoelastic and failure mechanical properties of the elastic fiber network of the inter-lamellar matrix in the annulus fibrosus of the disc. Acta Biomaterialia, 77, pp.292–300. doi:https://doi.org/10.1016/j.actbio.2018.07.023.

Urban, J.P. and Roberts, S. (2003). Degeneration of the intervertebral disc. Arthritis Research & Therapy, [online] 5(3), p.120. doi:https://doi.org/10.1186/ar629.

Vernon-roberts, B. And Pirie, C.J. (1977). Degenerative changes in the intervertebral discs of the lumbar spine and their sequelae. Rheumatology, 16(1), pp.13–21. Doi:https://doi.org/10.1093/rheumatology/16.1.13.

Verzijl, N., DeGroot, J., Zaken, C.B., Braun-Benjamin, O., Maroudas, A., Bank, R.A., Mizrahi, J., Schalkwijk, C.G., Thorpe, S.R., Baynes, J.W., Bijlsma, J.W.J., Lafeber, F.P.J.G. and TeKoppele, J.M. (2002). Crosslinking by advanced glycation end products increases the stiffness of the collagen network in human articular cartilage: A possible mechanism through which age is a risk factor for osteoarthritis. Arthritis & Rheumatism, 46(1), pp.114–123. doi:https://doi.org/10.1002/1529-0131(200201)46:1%3C114::aid-art10025%3E3.0.co;2-p.

Werbner, B., Lee, M., Lee, A., Yang, L., Habib, M., Fields, A.J. and O'Connell, G.D. (2022). Non-enzymatic glycation of annulus fibrosus alters tissue-level failure mechanics in tension. Journal of the Mechanical Behavior of Biomedical Materials, [online] 126, p.104992. doi:https://doi.org/10.1016/j.jmbbm.2021.104992.

www.sonsa.org. (n.d.). Intervertebral Discs» SONSA. [online] Available at: https://www.sonsa.org/spine-surgery/spine-anatomy/intervertebral-discs/#:~:text=The%20nucleus%20pulposus%20is%20the.

Zhou, M., Archibeck, E.S., Feteih, Y., Abubakr, Y. and O'Connell, G.D. (2023). Non-enzymatic glycation increases the failure risk of annulus fibrosus by predisposing the extrafibrillar matrix to greater stresses. Acta Biomaterialia, [online] 168, pp.223–234. doi:https://doi.org/10.1016/j.actbio.2023.07.003.

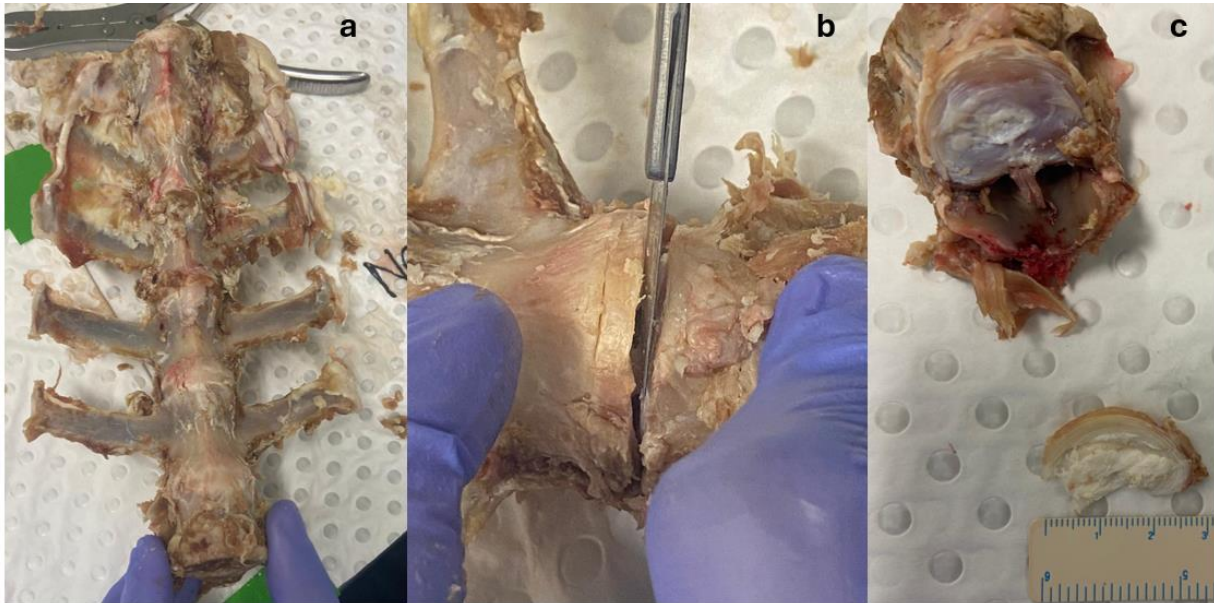# APPENDICES

Appendix A

- Isolation of sheep disc

Figure 1: (a) Sheep spine, (b) Identifying the IVD and making a cut horizontally to separate it, (c) The isolated sheep IVD

- Hand-held microtome

Figure 2: Parts of hand-held microtome

- Stress versus strain graph for the same specimen at the three different strain rates.
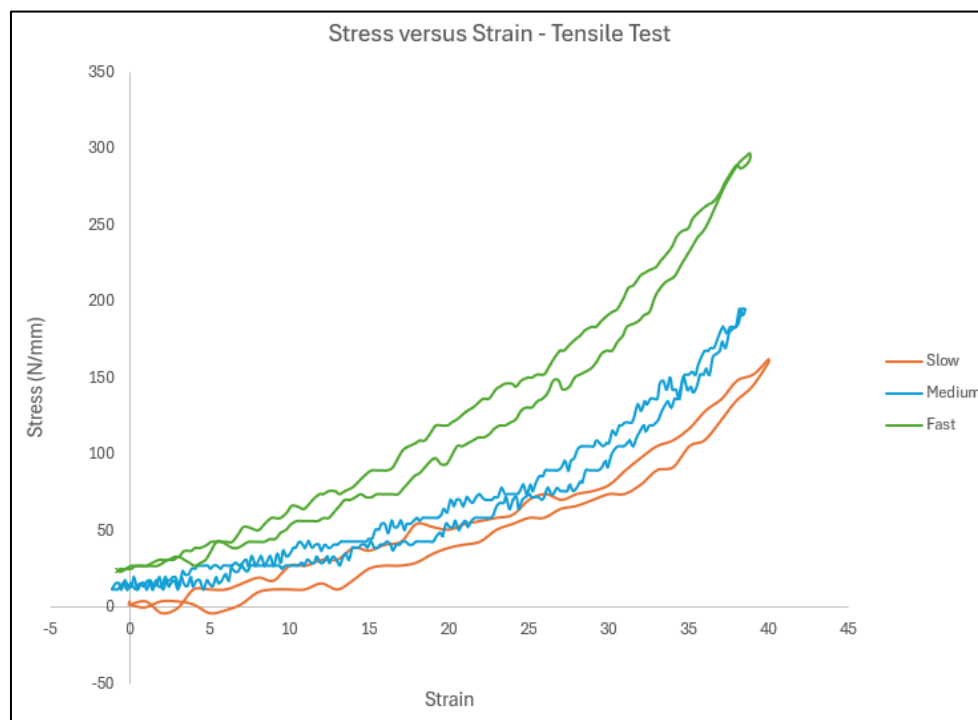
Figure 3: Stress versus strain graph

Appendix B

Testing Protocol

Disc isolation:

- The whole spine was thawed outside for 3 to 4 hours before the dissection.
- Then the disc level is chosen and using the thumb tracing along the IVD the CEP was identified.
- Slowly using a scalpel incision is made on the superior and inferior ends of the disc to detach it from the whole functional spinal unit.
- Use a bone cutter to remove the bone in the posterior side and make space. Keep making the incision bigger and isolate the disc from the spine.

Sample preparation and segmentation:

- After isolating the IVD they will be first frozen at $-20°C$ in the deep freezer.
- Then the frozen isolated IVD will be segmented into the required regions with the measurement of 5 mm (wide) using a scalpel blade making the cut at $90°$ angle to the ILM. For this research we will be mainly looking at the **PLT region**.

- After that the segmented IVD region will be wrapped in a gauze and PBS will be sprayed on it and stored in an air-tight container after labelling them.

- The next step will be to cut the segmented IVD region transversely for that masking tape will be lined circumferentially around the 3D printed platform of the hand-held microtome and then the sample will be kept in the middle and submerged in OCT compound and will be frozen at $-20°C$ within the microtome for 45 mins to 1 hour.

- Once it is ready, remove it from the freezer, remove the masking tape and slice into 1 mm (thickness) using a feather blade by turning the microtome two times accordingly to get the correct measurement.

- **Two slices** will be cut from each specimen as one slice each is required for tensile testing and shear testing. In total **12 slices** will be obtained from **six IVD samples (three samples each group).**

- PBS will be sprayed on to the sliced samples for the OCT compound surrounding it to dissolve.

Gripping of the sample using sandpaper:

- After the OCT compound is dissolved the sample is placed on a slide.

- Then four strips of sandpaper of the dimensions 6 mm (width) x 60 mm (length) were cut out from a 180-grit sandpaper sheet.

- Placing the sample slide under the microscope or magnifying glass to identify **two sets of functioning lamellae units**, i.e., two sets of ILM lying between two adjacent lamellae.

- Then applying the Loctite 480 glue, i.e., black dyed glue, on the edge of the sandpaper strips and evenly spreading it using a needle to remove the excess and then pressing the strips onto the sample carefully (2 mins drying time) and then flipping it doing the same step and sticking the other two sandpaper strips on the sample. (stick masking tape on one end of each sandpaper strip).

- Prepare the sample for tensile and shear testing such that when the strips are glued on the force applied will act in tensile direction for the first slice and in shear direction (90° to the position of the sample during tensile testing) for the second slice.

- Then the prepared samples will be transported to the CellScale testing machine in between two plates so that they don't get damaged.

Mechanical testing:

- Fill the CellScale bath with PBS and then release the prepared test sample into the bath and it will float because we have taped the distant ends, from the gripped specimen, of the sandpaper strips.
- Open the Labjoy software on the computer and open the required template from the set folder and name the file according to the given format.
- Lower the water bath and then reset the actuators.
- Measure the sample size, i.e., gripper to gripper distance, using a digital vernier calliper and set it in the system and then click move to size.
- Reduce the jog speed to 2 from 10 to have actuator control and obtain the correct distance between the actuators for the loading specimen. Then load the specimen onto the device using the two clamps given. Apply a preload of 100 mN.
- Then the specimen was subjected to dynamic tests (slow, medium, and fast tests), where the frequency for data acquisition was set as 1 Hz, 5 Hz and 100 Hz, respectively.
- Five cycles of dynamic loading were performed for each test and the specimens were stretched to 40% of their initial length at different strain rates, i.e., $0.1\,\%s^{-1}$, $1\,\%s^{-1}$, and $10\,\%s^{-1}$ for slow, medium, and fast tests, respectively for tensile and shear loading.
- After that at 100 Hz data recording and 10% of strain rate, failure test was performed.

Data and statistical analysis:

- The result from the CellScale machine gives force versus displacement data and force versus time data.
- That is copied onto the MS Excel template created and the graph between stress and strain of each point is plotted.
- Then using the line of best fit from the linear region of the loading curve stiffness is calculated.
- Using the stress and strain the area under the loading and unloading curve is obtained from which the hysteresis loss coefficient is calculated.
- For the failure test, obtain the peak load and energy absorbed at failure.
- Median and interquartile range was calculated for all values and graphs were plotted.

Appendix C

Formulas and calculations used for the finding the parameters

- **Stress**

$$\sigma = \frac{F}{A}$$

Where, F is the resultant force obtained after the displacement is applied

A is the cross-sectional area of the specimen

- **Strain**

$$\varepsilon = \frac{\Delta L}{L_o}$$

Where, ΔL is the change in the length, which is the difference between the initial length and final length

L_o is the initial length

- **Stiffness**

The gradient obtained from the slope equation of line of best from the linear region of the loading curve of the stress and strain relationship.

- **Maximum stress and peak force**

This is obtained by using the functions MAX(stress) and MAX(force) in the MS Excel template.

- **Energy absorbed and hysteresis loss coefficient**

These were found using the stress and strain values and calculating the area from which the area under the loading and unloading curves are calculated on the MS Excel template. Energy absorbed is the difference between the area under the loading curve and area under the unloading curve.

Hysteresis loss coefficient is the ratio of energy absorbed by the area under the loading curve.

Template for finding the stiffness and maximum stress
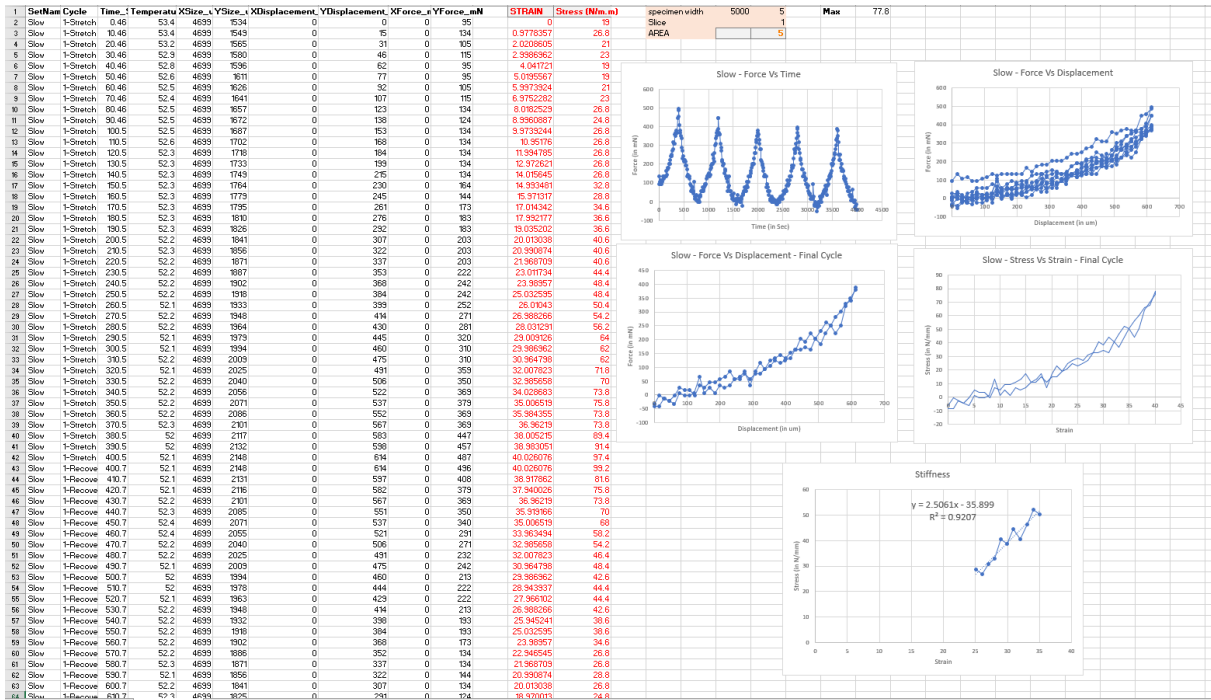
Template for finding the hysteresis loss coefficient and energy absorbed

Appendix D

Table 1: Maximum Stress of the Control Group

	control (Tension)			control (shear)		
Sample	**slow**	**medium**	**fast**	**slow**	**medium**	**fast**
GL1808864	48.4	56.2	56.2	134.6	150.2	210.8
GL1911504	19	58.2	111	93.4	138.4	89.4
GL1912463	77.8	48.4	140.4	269.6	412.4	502.4
Median	48.4	56.2	111	134.6	150.2	210.8

Table 2: Maximum Stress of the Diabetic Group

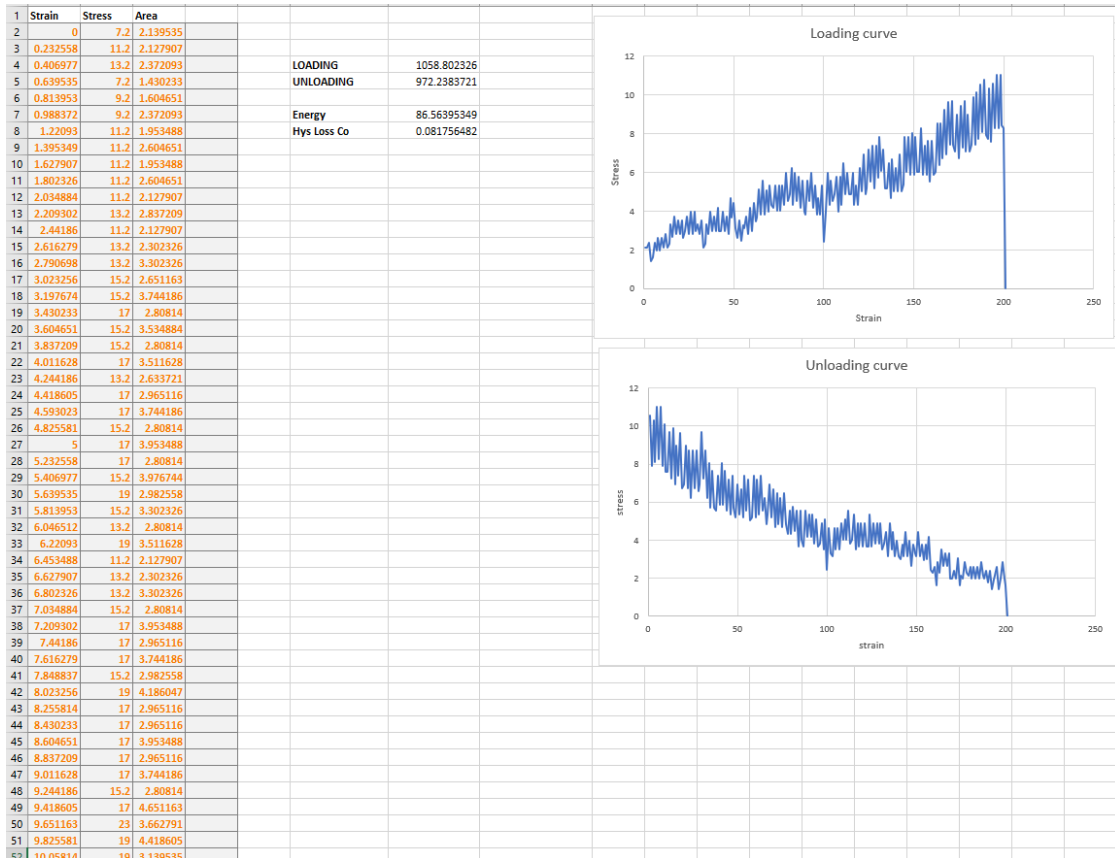|	Diabetic (Tension)			Diabetic (shear)		
Sample	**slow**	**medium**	**fast**	**slow**	**medium**	**fast**
GL1809052	134.6	189.4	269.6	50.4	32.8	44.4
GL1911447	162	195.2	297	19	77.8	118.8
GL1911471	58.2	48.4	73.8	26.8	64	85.6
Median	134.6	189.4	269.6	26.8	64	85.6

Table 3: Stiffness of the Control Group

	control (Tension)			control (shear)		
Sample	**slow**	**medium**	**fast**	**slow**	**medium**	**fast**
GL1808864	0.6967	0.5512	1.351	4.8899	5.7913	7.6148
GL1911504	0.4347	1.9128	4.1034	3.7953	4.6724	2.6376
GL1912463	2.5061	1.098	3.5918	11.885	16.952	18.891
Median	0.6967	1.098	3.5918	4.8899	5.7913	7.6148

Table 4: Stiffness of the Diabetic Group

	Diabetic (Tension)			Diabetic (shear)		
Sample	**slow**	**medium**	**fast**	**slow**	**medium**	**fast**
GL1809052	4.7397	6.4742	9.1907	1.573	0.5502	0.572
GL1911447	4.9189	7.4861	9.2447	0.5731	2.3105	3.0577
GL1911471	1.7824	0.77	2.0293	0.5879	2.2759	2.8627
Median	4.7397	6.4742	9.1907	0.5879	2.2759	2.8627

Table 5: Hysteresis Loss Coefficient of the Control Group

Sample	control (Tension)			control (shear)		
	slow	med	fast	slow	med	fast
GL1808864	0.09293	0.054774	0.01685	0.289747	0.260198	0.118093
GL1911504	0.272026	0.165338	0.149536	0.270089	0.213178	0.109306
GL1912463	0.115329	0.081756	0.082513	0.163634	0.1112	0.023546
Median	0.115329	0.081756	0.082513	0.270089	0.213178	0.109306

Table 6: Hysteresis Loss Coefficient of the Diabetic Group

Sample	Diabetic (Tension)			Diabetic (shear)		
	slow	medium	fast	slow	medium	fast
GL1809052	0.083005	0.0514835	0.153153	0.021882	0.064905	-0.02289
GL1911447	0.196277	0.1299171	0.139247	0.272026	0.320015	0.18392
GL1911471	0.08479	0.0523776	0.079541	0.183294	0.227307	0.089113
Median	0.08479	0.0523776	0.139247	0.183294	0.227307	0.089113

Table 7: Peak Load at Failure for the Control Group

Sample	control	
	Tension	shear
GL1808864	1974	1974
GL1911504	1113	3775
GL1912463	3530	6241
Median	1974	3775

Table 8: Peak Load at Failure for the Diabetic Group

Sample	Diabetic	
	Tension	shear
GL1809052	2943	2845
GL1911447	2004	2072
GL1911471	3041	761
Median	2943	2072

Table 9: Energy Absorbed at Failure for the Control Group

	control	
Sample	**Tension**	**shear**
GL1808864	42856.43	28957.29
GL1911504	3141.069	189748
GL1912463	36629.37	57926.01
Median	36629.37	57926.01

Table 10: Energy Absorbed at Failure for the Diabetic Group

	Diabetic	
Sample	**Tension**	**shear**
GL1809052	30508.02	240814.6
GL1911447	4902.956	91621.87
GL1911471	49565.74	36708.44
Median	30508.02	91621.87